Energy Storage Materials 77 (2025) 104195

Contents lists available at ScienceDirect

Energy Storage Materials

journal homepage: www.elsevier.com/locate/ensm

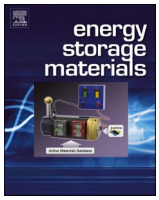

Long-lasting supercapacitor with stable electrode-electrolyte interface enabled by a biopolymer conjugate electrolyte additive

Seonghun Lee [a,1], Ji Young Park [a,1], Hyungsub Yoon [b,1], Jiyoon Park [c], Joohyung Lee [c], Byungil Hwang [d,*], Vinod V.T. Padil [e,*], Jun Young Cheong [f,*], Tae Gwang Yun [a,*]

[a] Department of Molecular Science and Technology, Ajou University, Suwon 16499, Republic of Korea
[b] Department of Intelligent Semiconductor Engineering, Chung-Ang University, Seoul 06974, Republic of Korea
[c] Department of Chemical Engineering, Myongji University, Yongin, Gyeonggi-do 17058, Republic of Korea
[d] School of Integrative Engineering, Chung-Ang University, Seoul 06974, Republic of Korea
[e] Amrita Vishwa Vidyapeetham, Amrita School for Sustainable Futures, Amrita University, Kollam, Kerala, India
[f] James Watt School of Engineering, University of Glasgow, Glasgow G12 8QQ, UK

ARTICLE INFO

Keywords:
Biopolymer conjugate electrolyte additive
Biopolymer-based supercapacitor
Stable electrode-electrolyte interface
Flexible lightweight electrode

ABSTRACT

Supercapacitor is one of most widely researched energy storage system because it stores more charge than capacitor and charges-discharges quicker than batteries. As surface reaction is prominent in the energy storage in supercapacitor, stable interface between electrode and electrolyte is a key to high performance. Although a formation of stable interface was achieved by surface modification of electrode and/or designing of novel materials/composites, they were limited by their complicated processing steps, costs, scalability, and eco-friendliness. In this work, we have firstly introduced a novel electrolyte additive composed of conjugated biopolymer of gum kondagogu/sodium alginate (KS), which is widely available and recyclable. At the KS concentration of 5 mg ml^{-1}, the capacitance retention improved from 58 % to 93 % for 30,000 cycles at a current density of 4.0 mA cm^{-2}, which was remarkable given the use of acidic H_2SO_4 electrolyte and carbon-based electrode. Postmortem analysis revealed the suitable concentration of KS necessary to ensure the interfacial protection as well as alleviation of side reactions by the introduction of KS, which can also be extended and scaled up in an industry scale.

1. Introduction

Amongst energy storage system, supercapacitor has been actively researched due its strong advantages in high power density and environmental friendliness (e.g., recyclability) [1–3]. The applications of supercapacitor include electronic devices, power supply, and electric vehicles, all of which are central to our daily lives [4–7]. In the supercapacitor, it is mainly governed by the surface-controlled reaction [8], in contrast to batteries where a diffusion-controlled reaction is also important. This means that an interfacial reaction between the electrode and electrolyte is an important contributor in determining the overall electrochemical performance. Therefore, building a stable interface between electrode and electrolyte is essential for ensuring a stable electrochemical performance in the supercapacitor.

Because the interfacial properties in the supercapacitor are important to ensure high electrochemical performance [9,10], many researchers have attempted diverse methods to improve & overcome the issues associated with them. For instance, Peng et al. employed an all-in-one integration of interface comprising of polyaniline-polyvinyl alcohol, which demonstrated an improved electrochemical performance [11]. Another study by Kang et al. employed a three-dimensional (3D) printing technology with a self-healable ink which greatly improved the interface between electrode and electrolyte [12]. Surface modification of the electrode was also shown to improve the interfacial properties in the supercapacitor. The atomic layer deposition method was carried out to coat a dielectric thin film on the electrode [13], which showed a remarkable 83 % capacitance retention even after 20,000 cycles. Tavinkumar et al. introduced a rationally designed core-shell

* Corresponding authors.
E-mail addresses: bihwang@cau.ac.kr (B. Hwang), vinodvtp@am.amrita.edu (V.V.T. Padil), JunYoung.Cheong@glasgow.ac.uk (J.Y. Cheong), ytk0402@ajou.ac.kr (T.G. Yun).
[1] These authors contributed equally to this work.

https://doi.org/10.1016/j.ensm.2025.104195
Received 31 January 2025; Received in revised form 10 March 2025; Accepted 21 March 2025
Available online 22 March 2025

structure comprising of $NiCo_2O_4/MoO_2$, which was further coated with NiO by atomic layer deposition method [14]. The resultant NiO-coated core-shell structure led to improved cycling stability as well as specific capacitance. Recently, ultrasonication-assisted synthetic method was employed to synthesize a Fe_3O_4/reduced graphene oxide composite electrode [15], which also showed a high capacitance of 169.2 F g^{-1} at 1.0 A g^{-1}. Nevertheless, all previously attempted approaches had significant limitations in i) scalability, ii) multiple processing steps, iii) cost of methodology, and/or iv) eco-friendliness, further preventing them from practical exploitation/commercialization on an industry scale. It is indispensable to come up with a sustainable solution that meets all of the abovementioned criteria and still achieves the high energy/power density supercapacitor for a long-term operation. Recently, the introduction of additives into electrolytes in energy storage systems has attracted considerable attention as an effective and convenient strategy to enhance electrolyte stability and form a stable electrode-electrolyte interface, thereby achieving long-term cycling stability, which is beneficial for scalability [16–18].

In this study, we have adopted a novel aqueous electrolyte system composed of H_2SO_4 solution and conjugated gum kondagogu (*Cochlospermum gossypium*)/sodium alginate (denoted as KS) additive, which led to the formation of surface protective layer on the surface of the electrode. The rheological properties and ionic conductivity of a novel aqueous electrolyte system were examined at various concentrations of KS additives. Using a symmetric supercapacitor based on carbon-based electrode and H_2SO_4 electrolyte, the effect of KS additive was further examined (denoted as KS-based supercapacitor). In comparison with the conventional H_2SO_4-based supercapacitor (denoted as W/O KS), the introduction of KS additive (at a concentration of 5 mg ml^{-1}) led to significantly improved capacitance retention (93 % capacitance retention for 30,000 cycles at a current density of 4.0 mA cm^{-2} improved from 58 %) and less byproducts on the surface of electrode. This is the earliest report on significant improvement of the long-term operation of the supercapacitor simply by introducing a biopolymer conjugate electrolyte additive, which has the potential to be exploited for commercialization due to its simple, low cost, environmentally friendly, applicable for large-scale production merits.

2. Results and discussion

2.1. Optimal design of KS/CNT electrode and KS additive for optimizing the electrochemical performance and reliability

We designed a conjugated KS composite structure for a highly stable supercapacitor offering biocompatibility and excellent mechanical/electrochemical reliability (Fig. 1a). Sodium alginate (SA), a natural anionic polysaccharide, contains sodium ions that can improve ionic conductivity in the electrolyte. Gum kondagogu is a natural polysaccharide that provides excellent viscosity control and stabilizing properties, which help disperse and support conductive fillers. The uniform dispersion of multi-walled carbon nanotubes (MWCNTs) within the KS matrix is crucial for enhancing the electrochemical performance of KS/CNT composite electrodes. By utilizing an aqueous cetyltrimethylammonium (CTAB) solution followed by ultrasonication, nanotube agglomeration was effectively prevented, resulting in the formation of a continuous percolation network of MWCNTs. This network substantially improved the electrical conductivity of electrodes by enabling more efficient electron transport during charge-discharge cycles. Additionally, prolonged air drying (48 h at room temperature) strengthened the bonding and adhesive properties of KS, resulting in a robust free-standing nanocomposite. This enhanced structural integrity played a pivotal role in maintaining both mechanical and electrochemical stability under repeated charge-discharge cycles. To further protect the KS matrix from dissolution in aqueous electrolytes, a trichloromethyl silane (TCMS) coating was applied via chemical vapor deposition (CVD) [19]. Even, after extended immersion in an aqueous electrolyte, the KS/CNT electrode retained its original morphology, confirming the effectiveness of the TCMS layer in preserving high structural stability (Fig. S1). Additionally, the average total electrode mass of the fabricated KS/CNT electrodes was 16.9 ± 0.03 mg for an identical area (1.13 cm^2), and the thickness was consistently measured as 0.16 mm across all samples, indicating excellent uniformity (Fig. S2). Ultimately, the fabricated KS/CNT composite electrode can serve as a free-standing electrode that offers both structural stability and electrochemical reliability (Fig. 1b and Fig. S3).

The lightweight property of the KS/CNT electrode was further highlighted by comparing its volumetric weight to that of commonly used substrates in energy storage systems, including metal-based materials, plastic film, and paper (Fig. S4). Specifically, The KS/CNT electrode exhibits an ultralight volumetric weight of 0.935 g cm^{-3}, which is nearly equivalent to that of commercial paper (0.926 g cm^{-3}) and significantly lower than polyethylene terephthalate (PET) film (1.366 g cm^{-3}), stainless-steel mesh (2.485 g cm^{-3}), zinc metal foil (3.441 g cm^{-3}), and titanium metal foil (3.626 g cm^{-3}). Since the KS/CNT electrode itself incorporates the active material (MWCNTs), it can function without the need for an additional inactive substrate layer, thus maintaining a lower overall mass. By contrast, conventional electrodes using heavier substrates further increase the total weight. The lightweight of the KS/CNT electrode is therefore advantageous for improving the energy density and mechanical flexibility, particularly in wearable energy storage applications.

Additionally, to improve electrochemical reliability via uniform surface-controlled reactions, we introduced a KS-based electrolyte additive. Although high electrical conductivity and low density of the KS/CNT electrodes enhance electrochemical performance, the long-term charge-discharge cycles lead to the formation of byproducts on the electrode surface and delamination of MWCNTs. Both phenomena degrade the overall electrochemical reliability. To address these issues, including the decline in electrochemical stability and the increased viscosity of the electrolyte, we designed a spongy KS-based electrolyte additive with ultra-low density, three-dimensional porosity, and a lightweight architecture (Fig. 1c). This spongy KS additive can remain in liquid form without significantly increasing viscosity of the electrolyte and readily dissolves in an aqueous solution. In addition, the sodium ions within the KS additive framework enhance the ionic conductivity of electrolyte, while the dissolved KS additive forms a thin protective layer on the electrode surface during charge-discharge cycles, thereby further improving electrochemical stability (Fig. 1d). Therefore, to clearly illustrate the advantages of our KS additive method over existing surface modification methods, we compared the electrochemical performance of our KS-based supercapacitors with previously reported interface enhanced supercapacitors (Table S1). The KS-based electrolyte additive demonstrated significantly higher ionic conductivity and improved cycle stability at lower additive concentrations compared to other existing methods. Moreover, the simple fabrication process and biopolymer-based composition of the KS additive method effectively overcome critical limitations of current approaches, including complicated processing steps, high costs, limited scalability, and low eco-friendliness (Fig. S5). These results clearly demonstrate the strong potential of the KS additive method for large-scale and sustainable industrial applications.

2.2. Morphological and chemical analysis of KS/CNT electrode and KS additive

To evaluate the uniformity, structural stability, and surface functionality of the KS/CNT electrode, we carried out internal structure and surface analyses. Initially, scanning electron microscope (SEM) was performed to examine the surface morphology of the electrode and the dispersion of MWCNTs (Fig. S6). The SEM images reveal that MWCNTs are uniformly dispersed throughout the KS/CNT composite, providing an effective electrical percolation pathway and reinforcing its

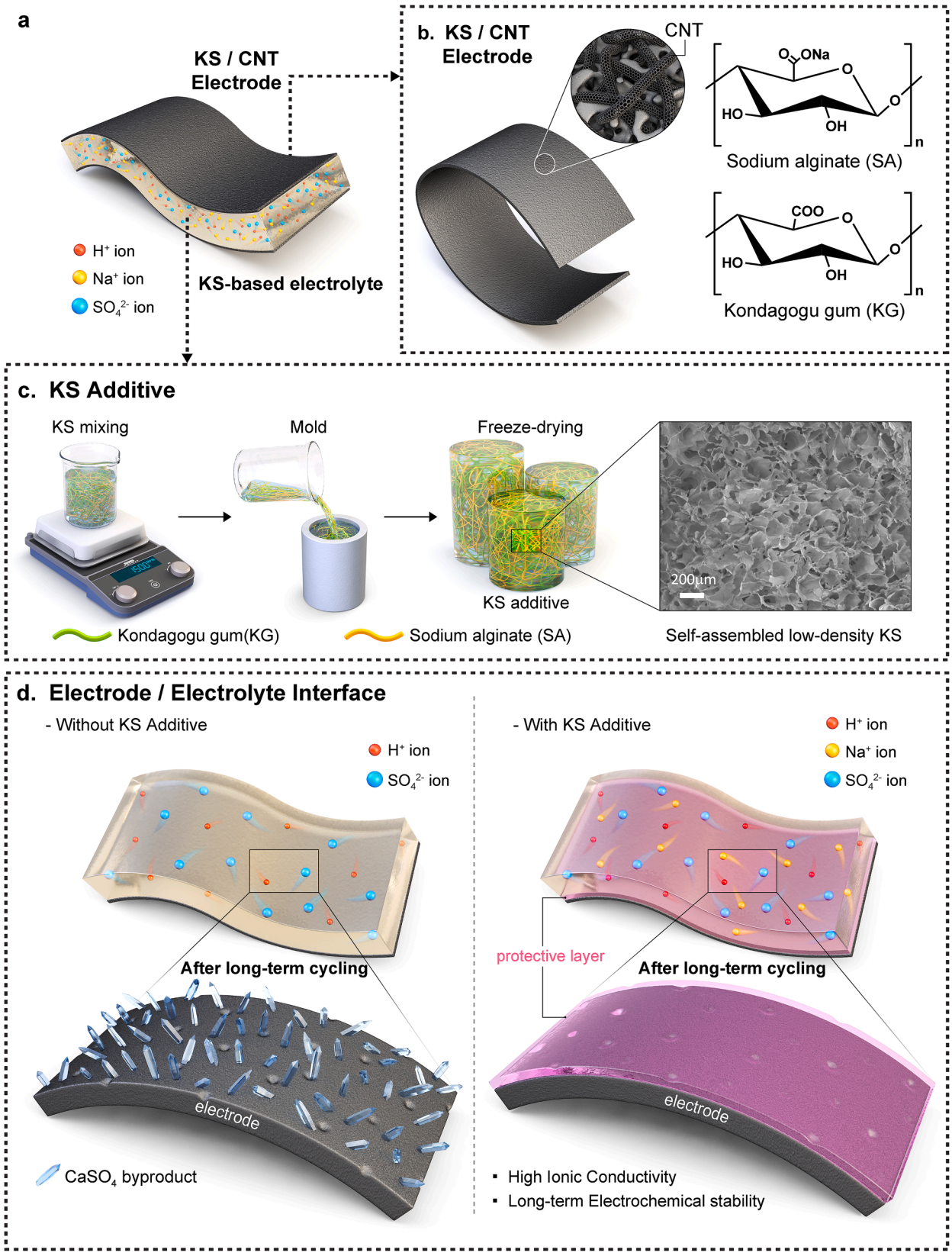

Fig. 1. Schematic of the KS-based supercapacitor. Schematic representations of a) the KS-based supercapacitor, b) KS/CNT electrode, and c) fabrication process of the KS additive via freeze-drying. d) Illustration showing the interface between the KS/CNT electrode and the electrolyte after long-term charge-discharge cycles.

mechanical stability. In addition, the electrode can be folded into various shapes without cracking, demonstrating its potential applicability in wearable energy storage applications (Fig. S7).

Next, we employed X-ray photoelectron spectroscopy (XPS) to confirm the TCMS coating on the electrode surface, which prevents water-induced dissolution (Fig. 2a-b). As indicated in the XPS spectra, the intensity of C—C and C—H bonds, abundant in both the KS and CNT, exhibited the highest values, along with peaks indicating polar functional groups such as -OH, C = O, C—O—C, and C—O. Notably, a Na 1s peak originating from SA was also detected (Fig. S8). The presence of Si 2p peaks further substantiated the uniform coverage of the TCMS layer on the electrode surface (Fig. S9).

To analyze the effect of the KS additive in electrolyte for the KS/CNT electrode, we carried out XPS and Fourier transform infrared spectroscopy (FT-IR) analyses at various KS concentrations (0–20 mg ml^{-1}) (Fig. 2c-d). After immersing the KS/CNT electrode in a KS-based electrolyte and then drying, we observed that the Si 2p peak intensity decreased at higher KS concentrations (Fig. 2c and Fig. S10). This suggests that a thicker KS-derived layer had formed on the electrode surface, highlighting the need to optimize KS additive concentration to prevent byproduct formation or MWCNTs delamination while still preserving beneficial surface reactions. Moreover, the gradual increase in carbon (C) and sodium (Na) peaks at higher KS concentrations suggests additional polysaccharide functional groups contributed by the KS additive (Fig. S11 and Table S2).

Additionally, FT-IR analysis provided further evidence of the effect of the KS-based electrolyte on the KS/CNT electrode (Fig. 2d and Table S3). In the absence of H_2SO_4 electrolyte, the KS/CNT electrode exhibited characteristic bands corresponding to O—H stretching (3360 cm^{-1}), C—H stretching (2920 cm^{-1}), O = C = O stretching (2362 cm^{-1}), C—O stretching (1015 cm^{-1}), C = O stretching (1722 cm^{-1}), and C = C stretching (1630 cm^{-1}), as well as Si-CH_3 bending/stretching bands (1267 cm^{-1} and 772 cm^{-1}). However, after immersion in electrolytes containing KS at various concentrations, the O—H stretching peak shifted slightly from 3375 cm^{-1} (W/O KS) to 3368 cm^{-1} (1 mg ml^{-1}, KS-1), 3370 cm^{-1} (5 mg ml^{-1}, KS-5), and 3372 cm^{-1} (20 mg ml^{-1}, KS-20). This minor red shift (i.e., to lower wavenumbers) is consistent with mild or partial hydrogen-bond formation at the electrode-electrolyte interface, rather than a strong hydrogen bond (which would typically produce a more pronounced shift). In other words, this minor red shift suggests that the KS additive promotes weak hydrogen bonding among O—H groups, rather than the strong interactions that would result in a significant spectral shift. This slight change implies an increase in O—H bonding interactions and the formation of a KS-based layer on the electrode surface [20]. Overall, these results indicate that the KS-containing electrolyte helps form a protective interfacial layer on the KS/CNT electrode, thereby contributing to improved electrochemical stability.

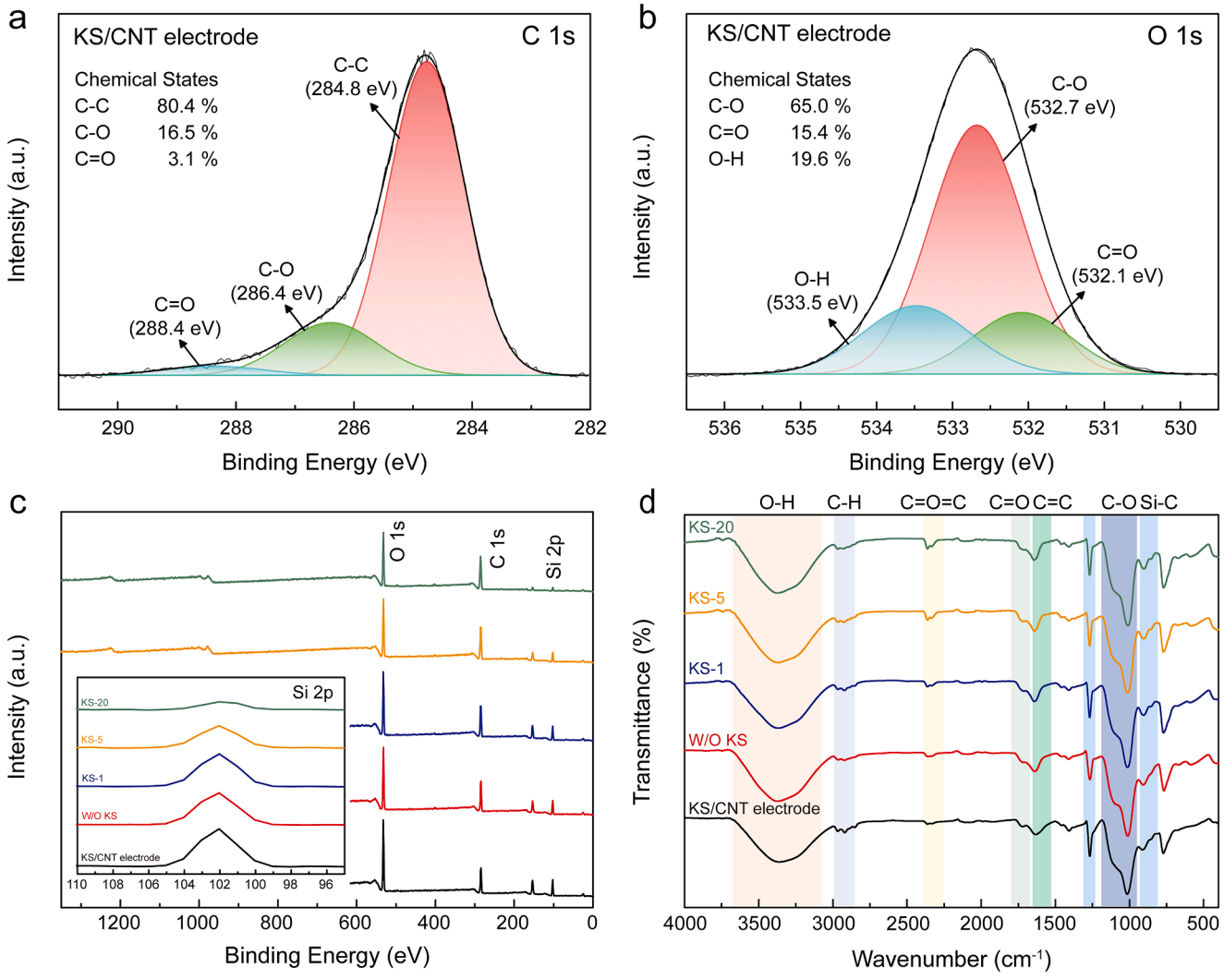

Fig. 2. Chemical properties of KS/CNT electrode and KS additive. X-ray photoelectron spectroscopy (XPS) analysis of the chemical composition of the KS/CNT electrode: a) C 1s and b) O 1s spectra. KS/CNT electrode in KS-based electrolyte: c) XPS analysis and d) Fourier transform infrared spectroscopy (FT-IR) spectrum.

2.3. The correlation between the ionic conductivity and viscosity of KS-based electrolyte

Introducing the KS electrolyte additive changes the properties of the aqueous electrolyte through the dissolution of KS, which in turn affects its electrochemical performance. As the KS concentration increases, two main effects emerge: (i) ionic conductivity increases due to the dissolution of sodium ions from the KS framework, and (ii) the viscosity of the aqueous electrolyte also increases because of the higher concentration of additives (increased solid content). This effect notably reduces ion mobility, leading to increased overpotential and subsequent electrochemical performance degradation [21]. Therefore, determining the optimal KS concentration is crucial for maximizing electrochemical performance. To investigate this concentration-dependent effect, we analyzed the correlation between ionic conductivity and viscosity in electrolytes containing various KS concentrations (Fig. 3). The ionic conductivity was measured via electrochemical impedance spectroscopy (EIS) testing using a stainless-steel symmetric cell (Fig. 3a), and the results were utilized to calculate the ionic conductivity of electrolyte (Fig. 3b). The ionic conductivity increases linearly as the KS concentration approaches 5 mg ml^{-1} (KS-5), as the sodium ions contained within the KS polysaccharide structure dissolve and contribute to the overall charge transport of the electrolyte. In contrast to gel-type electrolytes which often have limited ion mobility due to their cross-linked polymer matrices, the KS-based electrolyte retains a predominantly fluidic medium, allowing for higher ionic conductivity. However, beyond this critical threshold, the electrolyte becomes saturated with sodium ions and the associated increase in viscosity begins to outweigh the benefits of the increased sodium ions content, leading to saturation in ionic conductivity. These findings indicate that the optimal KS concentration range in which the supplementary sodium ions dissolved in the polysaccharide structure to enhance ionic conductivity lies within KS-5.

Changes in fluid behavior at various KS concentrations were observed to evaluate their impact on the viscosity of the electrolyte (Fig. 3c). As the KS concentration increased, the apparent electrolyte viscosity increased with the notably increased non-Newtonian behavior. The shear-rate-dependence of the viscosity, which is an indication of the degree of structuring of a fluid, became particularly severe at a KS concentration above 5 mg ml^{-1}, where the low-shear viscosity increased logarithmically. These changes in fluid behavior due to KS concentration directly impact ion mobility and diffusion coefficients. To investigate the correlation between KS concentration in the electrolyte and ion mobility, the EIS was measured using a KS/CNT electrode symmetric cell

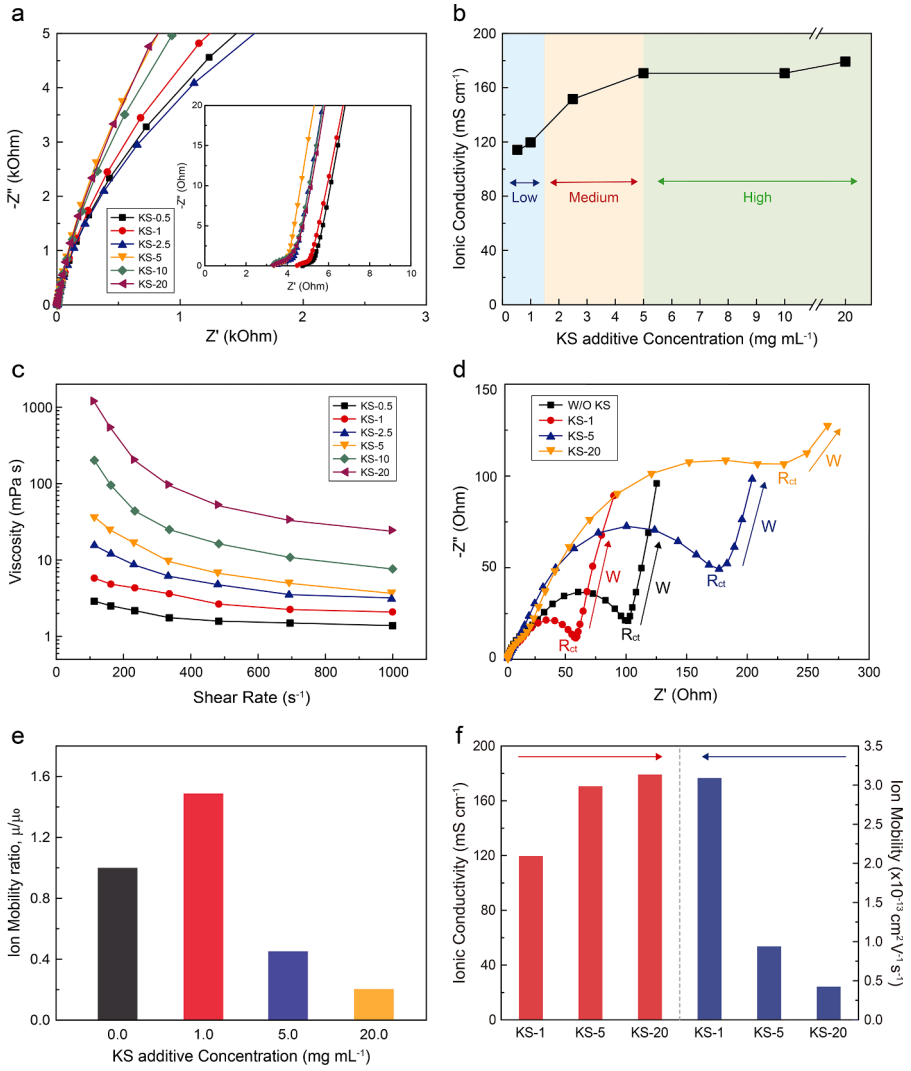

Fig. 3. Viscosity and ionic conductivity properties of the KS-based electrolyte. a) Electrochemical impedance spectroscopy (EIS) measurement using non-active stainless-steel electrodes and b) ionic conductivity in Nyquist plots at various KS additive concentrations. c) Analysis of fluid behavior (viscosity). d) EIS characterization of KS-based supercapacitor and e) ion mobility in Nyquist plots. f) Correlation between ionic conductivity and ion mobility with respect to the KS additive concentration.

(Fig. 3d). Based on the Nyquist plot from EIS measurements, the KS/CNT electrode with KS-1 exhibited the lower charge transfer resistance (R_{ct}) compared to that with W/O KS due to supplementary ions from KS additive. However, although the number of ions was increased by adding KS additive, the electrode with KS-5 and KS-20 showed the increased R_{ct} KS concentration. As the protective layer formed by KS on the electrode surface decreased the electrical conductivity of the KS/CNT electrode, charge transfer was impeded compared with electrode having W/O KS and KS-1. Furthermore, Warburg impedance slope, diffusion resistance of ions in electrolyte, was gradually decreased as KS concentration was increased, which means that the ion movements was impeded. It was attributed to the fact that the solid content of the salt/material in the electrolyte increased when KS additive was introduced. Therefore, due to increased viscosity of electrolyte, increased diffusion resistance of ions was inevitable, which was a consistent result with previous research [22–25].

To quantify the effect of KS concentration on electrochemical behavior, we calculated ion mobility based on Nernst-Einstein Eq. (1):

$$\mu = \frac{e\lambda^2\omega_2}{k_B T} \quad (1)$$

Where μ is ion mobility ($cm^2\ V^{-1}\ s^{-1}$), λ is the thickness of the electrical double layer (cm), ω_2 is the angular frequency corresponding to the minimum in the imaginary impedance (s^{-1}), e is the electron charge, k_B is the Boltzmann constant, and T is the absolute temperature [26,27]. The ion mobility of KS-1 was 1.49 times higher than that of the electrolyte without KS additive (W/O KS), however, unfortunately, the ion mobility of KS-5 and KS-20 was 0.45 times and 0.2 times that of ion mobility of W/O KS, which was attributed to the increased viscosity comparable to quasi-solid state electrolyte (Fig. 3e, Fig. S12, and Table S4). The increase in KS concentration in the electrolyte inevitably leads to higher viscosity, which in turn hinders ion movement, resulting in a decrease in the ion mobility and diffusion coefficient of the electrolyte. Consequently, the KS additive addition in electrolyte is beneficial to enhance the ionic conductivity of the electrolyte, while it increases the viscosity of the electrolyte, reducing ion mobility at high KS concentration (Fig. 3f). Therefore, to optimize the electrolyte with KS additive, we conducted electrochemical characterization with the KS-1, KS-5, and KS-20, represented low, medium, and high concentration region, respectively.

2.4. Electrochemical performance

To maximize the electrochemical performance by optimizing the KS concentration within the electrolyte, we assessed the electrochemical properties of KS/CNT electrodes utilizing an electrolyte with KS additive. Evaluation of the electrochemical characteristics was conducted through galvanostatic charge-discharge (GCD), cyclic voltammetry (CV) (Fig. 4). Under GCD tests at a current density of 0.2 mA cm^{-2}, the discharge time of KS/CNT electrode with KS-1 exhibited a negligible difference compared with the electrode W/O KS, while the electrode with higher KS concentration (KS-5 and KS-20) showed shorter discharge time, which means that the capacitance gradually decreased as KS concentration increased (Fig. 4a and Fig. S13). The areal capacitance depending on KS concentration was 17.9 mF cm^{-2}, 17.22 mF cm^{-2}, 15.7 mF cm^{-2}, and 13.6 mF cm^{-2}, corresponding to W/O KS, KS-1, KS-5, and KS-20, respectively. This was due to the gradual increase in viscosity of electrolytes with increasing KS concentration, which resulted in a decrease in ion mobility. Interestingly, the KS/CNT electrode with KS-1 exhibited a higher areal capacitance at a faster current density of 1.0 mA cm^{-2} than the W/O KS (Fig. S14). This was attributed to the fact that supplementary ions from KS prevented areal capacitance loss and improved electrochemical reversibility, when a fast current density was applied. In contrast, the relatively higher viscosity of the KS-5 and KS-20 electrolytes negates the benefits of supplementary ions form KS. Further insight into the effect of KS concentration on electrochemical performance was gained through CV tests. At a scan rate of 50 mV s^{-1}, the KS-1 exhibited the largest enclosed area among KS concentrations (Fig. 4b). When the areal capacitance was calculated based on CV tests, the KS-1 exhibited higher areal capacitance and outstanding electrochemical

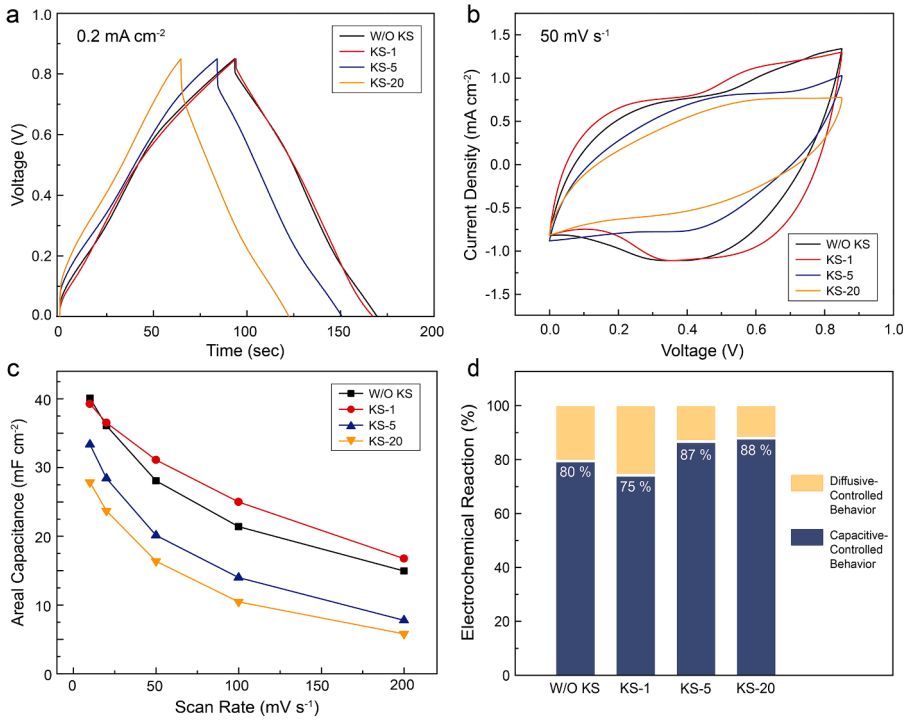

Fig. 4. Electrochemical properties of the KS-based supercapacitor at various KS additive concentrations. a) Galvanostatic charge-discharge (GCD) curves at a 0.2 mA cm^{-2}, b) cyclic voltammetry (CV) profiles at a scan rate of 50 mV s^{-1}, and c) areal capacitance at current densities in the range of 0.1–1.0 mA cm^{-2}. d) Deconvolution analysis of the electrochemical behavior of the KS-based supercapacitor.

reversibility (Fig. 4c and Fig. S15). Especially, at a scan rate of 50 mV s^{-1}, the areal capacitances in descending order were KS-1 (32 mF cm^{-2}), W/O KS (28 mF cm^{-2}), KS-5 (20 mF cm^{-2}), and KS-20 (16 mF cm^{-2}), which is attributed to the viscosity of the electrolytes, as mentioned above.

Additionally, the electrochemical behavior was analyzed to scrutinize the effect of KS concentration in energy storage mechanism by plotting the peak current in CV curves at various scan rates based on followed Eq. (2):

$$i = av^b \tag{2}$$

Where v is the scan rate, i the peak current, and b the electrochemical behavior (Fig. S16). Based on electrochemical behavior (b-value), where the ideal capacitive-controlled behavior is 1.0 and the diffusion-

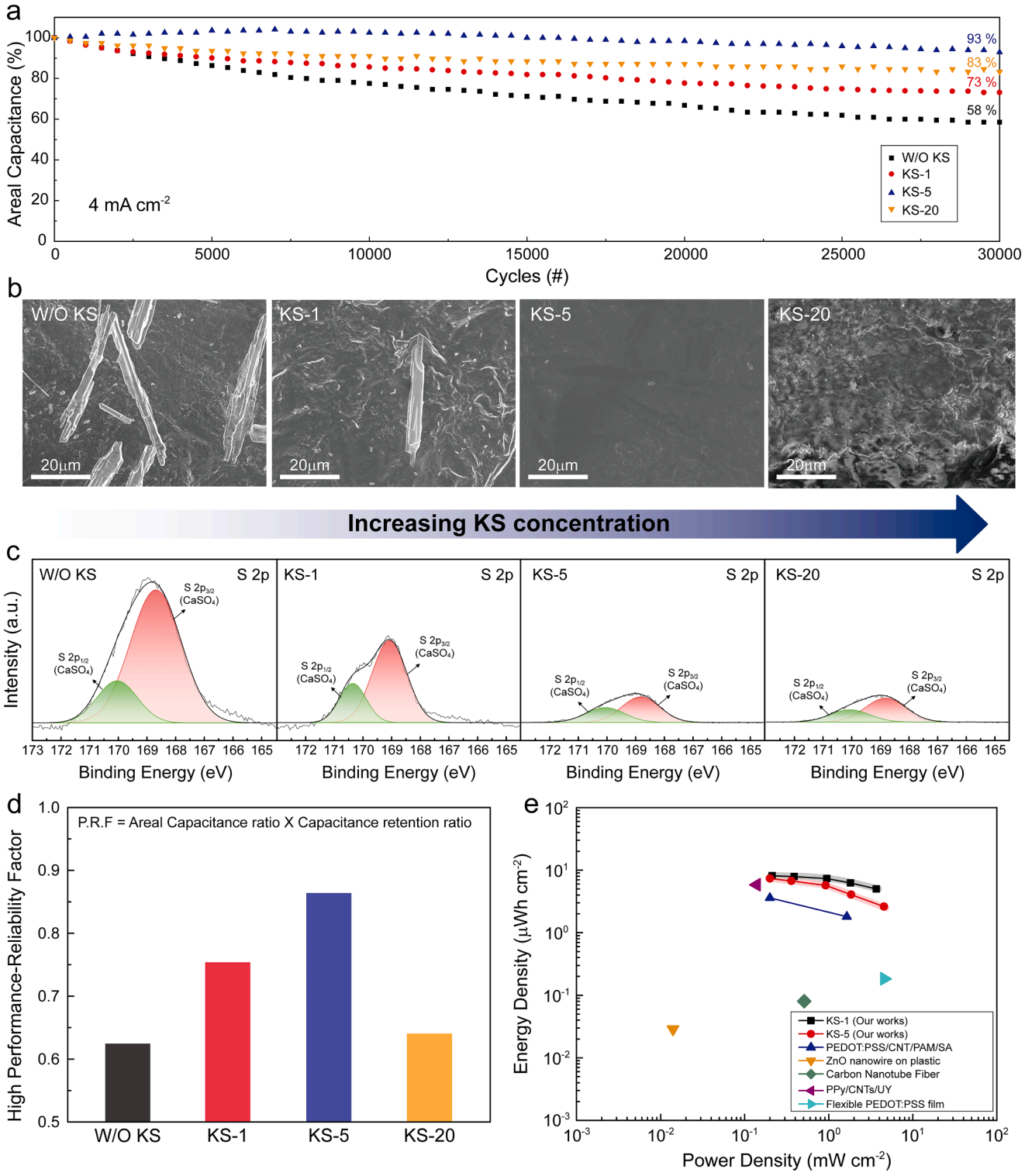

Fig. 5. Electrochemical reliability of the KS-based supercapacitors. a) Electrochemical reliability testing of 30,000 cycles at a current density of 4.0 mA cm^{-2}. b) SEM image and c) XPS analysis of electrode surfaces showing byproduct formation after charge-discharge cycling. d) High Performance-Reliability Factor (P.R.F) as a function of KS concentration. e) Electrochemical performance comparison with previously reported literatures based on the Ragone plot.

controlled behavior is 0.5, the KS-based supercapacitors mainly followed the ideal capacitive-controlled behavior with some degree of diffusion-controlled behavior. To accurately analyze the electrochemical behavior with a percentage, we calculated polynomial function (Eq. (3)) as below, where v term is ideal capacitive-controlled behavior and $v^{1/2}$ term is ideal diffusion-controlled behavior (Fig. 4d).

$$i(v) = k_1 v + k_2 v^{1/2} \quad (3)$$

Based on the calculated percentage of each KS concentration, KS-1 ranked the highest diffusion-controlled contribution fraction (25 %), followed by W/O KS (20 %), KS-5 (13 %), and KS-20 (12 %). Consistent with these findings, the CV curves in W/O KS and KS-1 electrolytes exhibited pseudo-capacitive behavior with broad-enclosed area, whereas KS-5 and KS-20 showed more symmetric profiles typical of electrical double layer behavior (Fig. S15). The results suggested that the diffusion-controlled behavior plays a critical role in the areal capacitance enhancement.

2.5. Electrochemical reliability

To evaluate the electrochemical reliability of KS-based supercapacitors, we performed long-term charge-discharge cycling tests at a current density of 4.0 mA cm^{-2} under controlled conditions (temperature: 25 °C, relative humidity: 50 %) (Fig. 5a). The KS-5 demonstrated the highest areal capacitance retention (93 %) after 30,000 charge-discharge cycles, followed by KS-20 (83 %), KS-1 (73 %), and W/O KS (58 %). This result indicates that higher KS concentrations effectively sustain electrochemical performance by forming a protective layer that reduces delamination of the active material. SEM images of the electrode surface after 30,000 charge-discharge cycles confirm this protective effect (Fig. 5b). In the absence of KS additive (W/O KS), the calcium ions originally utilized as ionic cross-linkers in the KS/CNT electrode reacted with SO_4^{2-} ions from the electrolyte, leading to the nucleation and growth of crystalline byproducts ($CaSO_4$). Over repeated charge-discharge cycling, these insoluble crystals progressively grew, locally consumed ions, and ultimately promoted delamination of the active material from the electrode surface, significantly impairing long-term electrochemical reliability. X-ray diffraction (XRD) patterns of cycled W/O KS electrode clearly exhibited diffraction peaks corresponding to $CaSO_4 \bullet 2H_2O$ (PDF #33–0311) (Fig. S17), and energy dispersive X-ray spectroscopy (EDS) elemental mapping further confirmed the presence of calcium and sulfur, indicating the formation of $CaSO_4 \bullet 2H_2O$ (Fig. S18). However, the addition of KS additive to the electrolyte resulted in the formation of a thin, uniform KS-based protective layer on the electrode surface, significantly suppressing byproduct formation. In KS-1, byproduct was reduced but still partially present, suggesting insufficient protection. In contrast, KS-5 formed a more uniformly protective layer, eliminating these byproducts and providing the excellent electrochemical reliability. At an even higher KS concentration (KS-20), a thick protective layer formed, which reduced electrical conductivity and thus lowered the overall electrochemical stability compared to KS-5. XPS analysis provided additional evidence supporting these observations (Fig. 5c, Fig. S19, and Fig. S20). As KS concentration increased, the intensities of S 2p and Ca 2p peaks corresponding to $CaSO_4 \bullet 2H_2O$ byproduct significantly declined, consistent with SEM and XRD results. These comprehensive analyses clearly demonstrate that an optimal KS additive concentration effectively prevents byproduct precipitation, thus enhancing long-term electrochemical reliability during repeated charge-discharge cycling.

Since a low KS concentration (e.g., KS-1) enhances ion mobility, leading to higher areal capacitance, while a high KS concentration (e.g., KS-5) facilitates the formation of a uniform protective interfacial layer, ensuring enhanced electrochemical reliability, determining the optimal KS concentration requires a balanced evaluation of both factors. Therefore, to systematically optimize KS concentration while considering both electrochemical performance and reliability, we introduced our newly defined high electrochemical performance-reliability factor (P.R.F), as shown below (Fig. 5d).

$$P.R.F = Ratio\ of\ areal\ capacitance \times Ratio\ of\ capacitance\ retention \quad (4)$$

The P.R.F factor provides a comprehensive assessment by integrating the key performance factors the ratio of areal capacitance, which was normalized based on the maximum areal capacitance, and the ratio of capacitance retention, which was normalized based on the capacitance retention after 30,000 charge-discharge cycles at a current density of 4.0 mA cm^{-2}. The P.R.F approach integrates both electrochemical performance and reliability, ensuring a balanced electrolyte design. As a result, KS-5 provides the optimal balance of electrochemical reliability (93 % capacitance retention after 30,000 cycles) and adequate areal capacitance (36.5 mF cm^{-2}), achieving the highest P.R.F value as the optimized concentration for enhancing overall supercapacitor performance.

To evaluate the electrochemical performance of our KS-based supercapacitor, the areal energy and power densities were calculated and compared with recently reported supercapacitors based on a Ragone plot (Fig. 5e and Table S5). The KS/CNT electrode with KS-1 exhibited areal power densities ranging 0.21–3.68 mW cm^{-2} and areal energy densities ranging 5.01–8.15 μWh cm^{-2}. Additionally, the KS/CNT electrode with KS-5 showed areal power densities ranging 0.2–4.55 mW cm^{-2} and areal energy densities ranging 2.6–7.33 μWh cm^{-2}. At the KS-5, ideal electrical double layer behavior was observed unlike the KS-1, resulting in an increased areal power density but a decreased areal energy density. Furthermore, as shown in the Ragone plot, the designed KS-based supercapacitors demonstrate higher areal energy and power densities compared with previously reported gel-type electrolyte and free-standing composite electrodes [28–32]. The KS-based supercapacitor exhibited improved areal energy and power densities compared with supercapacitors utilizing PAM/SA/Na_2SO_4-based hydrogel electrolyte (0.2–1.64 mW cm^{-2} and 3.6–1.8 μWh cm^{-2} of areal energy and power densities) [28], ZnO nanowire on plastic film (0.014 mW cm^{-2} and 0.027 μWh cm^{-2}) [29], and carbon nanotube fiber (0.493 mW cm^{-2} and 0.08 μWh cm^{-2}) [30]. Furthermore, compared to PPy/CNTs/urethane elastic fiber-based supercapacitors (0.133 mW cm^{-2} and 6.13 μWh cm^{-2}) [31] and flexible PEDOT:PSS-based supercapacitors (4.98 mW cm^{-2} and 0.183 μWh cm^{-2}) [32], KS-based supercapacitors exhibited higher areal energy and power densities. While these polymer-based supercapacitors exhibit excellent functionality, their areal energy and power densities are relatively lower.

Thus, the KS/CNT electrode and KS additive designed in this study were achieved through a simple process using inexpensive materials. The free-standing KS/CNT electrode is binder and substrate free, biocompatible, flexible, and can be manufactured in large-scale applications. By adding the KS additive to form a thin protective layer, the electrochemical reliability was improved even under long-term charge-discharge cycles and the device demonstrated improved electrochemical performance. Additionally, our previous studies have extensively evaluated the environmental characteristics of KS biopolymer composites, confirming their excellent biodegradability and recyclability. Specifically, KS-based sponges and films exhibited outstanding biodegradability (up to 92 % within 28 days) and high recyclability (91 %) [33, 34]. Thus, the high biodegradability and eco-friendly properties of the KS-based supercapacitor developed in this study highlight its strong potential for applications across various industries.

3. Conclusion

In summary, novel additive concept was firstly employed in the supercapacitor system to build a stable interface between electrode and electrolyte, leading to enhanced electrochemical reliability. With the introduction of conjugated KS, the protective layer is formed on the

surface of electrode, suppressing the formation of byproducts and facile ionic/electron transport. Even a slight addition of conjugated KS in the H_2SO_4-based electrolyte (in the range of 0.5–5 mg ml^{-1}) led to significantly improved interfacial properties and long-term operation (improving from 58 % to 93 % of capacitance retention for 30,000 cycles at a current density of 4.0 mA cm^{-2}), ideal for practical utilization of supercapacitors. Introducing a novel additive is straightforward, simple, and industrially applicable, which can be extended to the commercial production line used for producing the supercapacitor.

4. Experimental section

4.1. Materials

Gum kondagogu (*Cochlospermum gossypium*) was purchased from the Girijan cooperative society in India. Sodium alginate (SA), calcium chloride ($CaCl_2$, ≥ 93.0 %), trichloromethyl silane (TCMS), multi-walled carbon nanotubes (MWCNTs), cetyltrimethylammonium bromide (CTAB), and sulfuric acid (H_2SO_4) were purchased from Sigma-Aldrich Co. and used without further purification. Deionized water used in all of the experiments.

4.2. KS/CNT composite electrode preparation

The MWCNTs was dispersed with a CTAB (0.8:1.0 wt %) for 1 hour using an ultrasonic homogenizer (Sonopuls HD 3400, Bandelin, Berlin). Then, The Ca^{2+}-crosslinked KS solution (40:60 w/w) was added using a magnetic stirrer at a concentration of 15 % of MWCNTs dispersion based on the total gum kondagogu/sodium alginate weight for 2 h. After mixing, the final dispersion was dispensed into dishes and the solvent was left to evaporate at room temperature till it dried for 48 h. And then, in order to realize the structural stability of the KS/CNT composite electrode, a thin silane layer was deposited on the surface using chemical vapor deposition (CVD) for 30 min starting the reaction at 50 °C with TCMS at 65 % relative humidity. Then, the residual byproducts were removed through vacuum drying at 50 °C for 2 h [19].

4.3. Fabrication of electrolyte with KS additive

Gum kondagogu and sodium alginate 1.5 w/w % solution was completely mixed at a ratio of 1:1 w/w % and then stirred at room temperature at 1500 rpm for 2 h. After stirring, the resulting KS solution was poured into a mold and lyophilized at −80 °C for 72 h to prepare a KS additive [34,35]. 1 M H_2SO_4 aqueous solution was prepared, added to the solution at various KS additive concentrations (from 0 to 20 mg ml^{-1}), and stirred at room temperature for 30 min to prepare KS-based electrolyte.

4.4. Characterizations

Field-emission scanning electron microscope (FE-SEM, SIGMA 300 Carl Zeiss) was used to characterize the morphology of electrodes. Energy dispersive X-ray spectroscopy (EDS) coupled to FE-SEM was used to determine the chemical elements present in the byproducts on the electrode surface. Fourier transform infrared attenuated total reflection (FTIR-ATR) spectroscopy was used to determine the functional groups on the electrode in the range 400–4000 cm^{-1} on Nicolet iS50 (Thermo Fisher Scientific Instrument). In addition, the interaction between the electrode and the electrolyte according to the concentration of the KS additive was confirmed. The measurement of X-ray photoelectron spectroscopy (XPS) including the elements of C, O, Na, Si, S, and Ca was conducted on K-alpha (Thermo VG Scientific). In addition, XPS was used to determine the chemical composition of the samples and confirmed the formation of byproducts before and after charge-discharge cycles. To examine the presence of byproducts, X-ray diffraction (XRD) measurements were performed using Cu Kα radiation with a High Power X-Ray Diffractometer. XRD patterns were collected in the 2θ range between 10° and 60° with a scan speed of 5° min^{-1}.

4.5. Rheological characterization of electrolytes

The apparent viscosities of KS-based electrolyte solutions with various KS additive concentrations (0.5, 1.0, 2.5, 5.0, 10, and 20 mg ml^{-1}) were measured by using a Haake MARS 40 rheometer (Thermo Fischer Scientific) with parallel-plate geometry (diameter: 35 mm, gap distance: 0.1 mm). The measurements were performed in the shear rate range between 10^2 and 10^3 s^{-1}; during the measurements, a shear rate corresponding to each data point was maintained until the measured shear stress for the sample reached a plateau value, which was used to calculate the reported apparent viscosity.

4.6. Electrochemical characterization

For the electrochemical tests, CR2032-type coin cell was used with a symmetric electrode configuration with a voltage window between 0 and 0.85 V. electrode was prepared by punching a circular disk with a diameter of 12 mm. The electrolyte was composed of 1 M H_2SO_4 aqueous solution. All the electrochemical tests were performed using a BCS-805 (BioLogic) cell test system. Cyclic voltammetry (CV) tests, galvanostatic charge-discharge (GCD) tests, and electrochemical impedance spectroscopy (EIS) were conducted to measure the electrochemical properties of electrodes and electrolytes based on conjugated KS. The CV tests were conducted at scan rates of 0.01, 0.02, 0.05, 0.1, and 0.2 V s^{-1}, while the GCD tests were performed under current densities of 0.1, 0.2, 0.5, 1.0, and 2.0 mA cm^{-2}. The long-term charge-discharge cycles test was conducted with a current density of 4.0 mA cm^{-2} for 30,000 cycles under controlled environmental conditions: room temperature of 25 °C and relative humidity of 50 %. All electrochemical tests were conducted inside a controlled chamber to maintain these conditions consistently. EIS test was performed between 10 kHz to 100 mHz of frequency range with a voltage amplitude of 10 mV. We calculated the areal capacitance (C_a) using CV test and GCD test, and the following Eqs. (5–8) were utilized to calculate the areal energy density (E_a) and the power density (P_a). Here, i/A is the areal current density, μ is the scan rate, ΔV is the potential window, v is the potential, and t is the discharge time.

$$C_a = \int \frac{ivdv}{2\mu A \Delta V} \tag{5}$$

$$C_a = \frac{it}{A\Delta V} \tag{6}$$

$$E_a = \frac{1}{2} C_a (\Delta V)^2 \tag{7}$$

$$P_a = \frac{E_a \times 3600}{t} \tag{8}$$

The EIS test was used to measure ionic conductivity (σ) from Nyquist plot. Ionic conductivity was evaluated by impedance test of symmetric stainless-steel mesh. Impedance measurements were carried out between 100 kHz to 100 mHz of frequency range with a voltage amplitude of 10 mV using a ZIVE SP1 (WonAtech Co.). The following Eq. (9) was utilized to calculate ionic conductivity (σ). l is thickness (the distance between the stainless-steel meshes), A is area of the surface, and R_b is the bulk resistance.

$$\sigma = l\,(R_b A)^{-1} \tag{9}$$

CRediT authorship contribution statement

Seonghun Lee: Writing – original draft, Investigation, Data curation, Conceptualization. **Ji Young Park:** Writing – original draft,

Investigation, Data curation. **Hyungsub Yoon:** Writing – original draft, Investigation, Data curation. **Jiyoon Park:** Data curation. **Joohyung Lee:** Writing – review & editing. **Byungil Hwang:** Writing – review & editing, Supervision. **Vinod V.T. Padil:** Writing – review & editing, Supervision. **Jun Young Cheong:** Writing – review & editing, Supervision, Funding acquisition, Conceptualization. **Tae Gwang Yun:** Writing – review & editing, Supervision, Funding acquisition, Conceptualization.

Declaration of competing interest

The authors declare that they have no known competing financial interests or personal relationships that could have appeared to influence the work reported in this paper.

Acknowledgements

This research was supported by GRDC (Global Research Development Center) Cooperative Hub Program through the National Research Foundation of Korea (NRF) funded by the Ministry of Science and ICT (MSIT) (RS-2023–00257595). This work was also supported by the University of Glasgow Start-up Fund. Vinod V.T. Padil acknowledged the support through AMRITA Seed Grant (Proposal ID: ASG2022104), Amrita Vishwaya Vidyapeetham (Amrita University), India.

Supplementary materials

Supplementary material associated with this article can be found, in the online version, at doi:10.1016/j.ensm.2025.104195.

Data availability

Data will be made available on request.

References

[1] J. Dixon, I. Nakashima, E.F. Arcos, M. Ortuzar, Electric vehicle using a combination of ultracapacitors and ZEBRA battery, IEEE Trans. Ind. Electron. 57 (2010) 943–949, https://doi.org/10.1109/TIE.2009.2027920.

[2] L. Zhang, X. Hu, Z. Wang, F. Sun, D.G. Dorrell, A review of supercapacitor modeling, estimation, and applications: a control/management perspective, Renew. Sustain. Energy Rev. 81 (2018) 1868–1878, https://doi.org/10.1016/j.rser.2017.05.283.

[3] P. Thounthong, S. Rael, B. Davat, Control Strategy of Fuel Cell and Supercapacitors Association for a distributed generation system, IEEE Trans. Ind. Electron. 54 (2007) 3225–3233, https://doi.org/10.1109/TIE.2007.896477.

[4] K.K. Kar 1968, Handbook of Nanocomposite Supercapacitor Materials I: Characteristics, 1st ed., Springer International Publishing, Cham, 2020.

[5] C.R. Arunkumar, U.B. Manthati, S. Punna, Supercapacitor-based transient power supply for DC microgrid applications, Renew. Sustain. Energy Rev. 104 (2022) 463–472, https://doi.org/10.1007/s00202-021-01312-7.

[6] Ricardo Barrero, Xavier Tackoen, Joeri Van Mierlo, Improving energy efficiency in public transport: stationary supercapacitor based Energy Storage Systems for a metro network, 2008 IEEE Veh. Power Propuls. Conf. (2008) 1–8, https://doi.org/10.1109/vppc.2008.4677491.

[7] L. Guo, P. Hu, H. Wei, Development of supercapacitor hybrid electric vehicle, J. Energy Storage 65 (2023) 107269, https://doi.org/10.1016/j.est.2023.107269.

[8] J. Xie, P. Yang, Y. Wang, T. Qi, Y. Lei, C.M. Li, Puzzles and confusions in supercapacitor and battery: theory and solutions, J. Power Sources 401 (2018) 213–223, https://doi.org/10.1016/j.jpowsour.2018.08.090.

[9] W. Guo, C. Yu, S. Li, J. Qiu, Toward commercial-level mass-loading electrodes for supercapacitors: opportunities, challenges and perspectives, Energy Environ. Sci. 14 (2021) 576, https://doi.org/10.1039/d0ee02649b. –61.

[10] W. Kang, L. Zeng, S. Ling, C. Lv, J. Liu, R. Yuan, C. Zhang, Three-dimensional printed mechanically compliant supercapacitor with exceptional areal capacitance from a self-healable ink, Adv. Funct. Mater. 31 (2021), https://doi.org/10.1002/adfm.202102184.

[11] Y. Peng, W. Yuan, X. Liu, P. Xie, F. Yang, H. Zhao, D. Lu, Y. Yin, Z. Wu, All-in-one integration of polyaniline-polyvinyl alcohol electrode/electrolyte interface for tailorable solid-state supercapacitors, J. Energy Storage 61 (2023) 106701, https://doi.org/10.1016/j.est.2023.106701.

[12] W. Kang, L. Zeng, S. Ling, R. Yuan, C. Zhang, Self-healable inks permitting 3D printing of diverse systems towards advanced bicontinuous supercapacitors, Energy Storage Mater 35 (2021) 345–352, https://doi.org/10.1016/j.ensm.2020.11.032.

[13] Y. Bai, N. Li, C. Yang, X. Wu, H. Yang, W. Chen, H. Li, B. Zhao, P. Wang, X. Han, Realizing high-voltage and ultralong-life supercapacitors by a universal interfacial engineering strategy, J. Power Sources 510 (2021) 230406, https://doi.org/10.1016/j.jpowsour.2021.230406.

[14] T. Kavinkumar, S. Seenivasan, H.H. Lee, H. Jung, J.W. Han, D. Kim, Interface-modulated uniform outer nanolayer: a category of electrodes of nanolayer-encapsulated core-shell configuration for supercapacitors, Nano Energy 81 (2021) 105667, https://doi.org/10.1016/j.nanoen.2020.105667.

[15] B.J. Choudhury, K. Roy, V.S. Moholkar, Improvement of supercapacitor performance through enhanced interfacial interactions induced by sonication, Ind. Eng. Chem. Res. 60 (2021) 7611–7623, https://doi.org/10.1021/acs.iecr.1c00279.

[16] Z. Wang, C. Su, R. Xu, K. Li, B. Yang, T. Li, K. Chen, W. Xu, J. Chen, F. Li, B. Li, A. Hu, J. Long, Weak traction effect modulates anionic solvation transition for stable-cycling and fast-charging lithium metal batteries, Energy Storage Mater. 75 (2025) 104105, https://doi.org/10.1016/j.ensm.2025.104105.

[17] T. Li, K. Chen, B. Yang, K. Li, B. Li, M. He, L. Yang, A. Hu, J. Long, In situ polymerization of 1,3-dioxolane and formation of fluorine/boron-rich interfaces enabled by film-forming additives for long-life lithium metal batteries, Chem. Sci. 15 (2024) 12108–12117, https://doi.org/10.1039/d4sc02010c.

[18] B. Yang, A. Hu, T. Li, K. Li, Y. Li, J. Jiang, Z. Xiao, Z.W. Seh, J. Long, Eliminating water hazards and regulating electrode-electrolyte interfaces by multifunctional sacrificial electrolyte additives for long-life lithium metal batteries, Energy Storage Mater. 70 (2024) 103512, https://doi.org/10.1016/j.ensm.2024.103512.

[19] S. S R.K. Ramakrishnan, S. Palanisamy, N.S. Sumitha, A.K.K Padinjareveetil, S. Wacławek, T. Uyar, M. Černík, R.S. Varma, J.Y. Cheong, V. Vellora Thekkae Padil, Regenerable and ultraflexible sustainable film derived from tree gum kondagogu for high-performance electromagnetic interference shielding, ACS Sustain. Chem. Eng. 11 (2023) 7344–7356, https://doi.org/10.1021/acssuschemeng.2c07743.

[20] Y. Zhang, D. Wu, F. Huang, Y. Cai, Y. Li, H. Ke, P. Lv, Q. Wei, "Water-in-salt" nonalkaline gel polymer electrolytes enable flexible zinc-air batteries with ultra-long operating time, Adv. Funct. Mater. 32 (2022), https://doi.org/10.1002/adfm.202203204.

[21] H. Dai, G. Zhang, D. Rawach, C. Fu, C. Wang, X. Liu, M. Dubois, C. Lai, S. Sun, Polymer gel electrolytes for flexible supercapacitors: recent progress, challenges, and perspectives, Energy Storage Mater. 34 (2021) 320–355, https://doi.org/10.1016/j.ensm.2020.09.018.

[22] M. Saito, S. Kawaharasaki, K. Ito, S. Yamada, K. Hayamizu, S. Seki, Strategies for fast ion transport in electrochemical capacitor electrolytes from diffusion coefficients, ionic conductivity, viscosity, density and interaction energies based on HSAB theory, RSC Adv. 7 (2017) 14528–14535, https://doi.org/10.1039/c7ra00455a.

[23] A. Massaro, J. Avila, K. Goloviznina, I. Rivalta, C. Gerbaldi, M. Pavone, M.F. Costa Gomes, A.A.H. Padua, Sodium diffusion in ionic liquid-based electrolytes for Na-ion batteries: the effect of polarizable force fields, Phys. Chem. Chem. Phys. 22 (2020) 2114–2122, https://doi.org/10.1039/d0cp02760j.

[24] N. Yao, L. Yu, Z. Fu, X. Shen, T. Hou, X. Liu, Y. Gao, R. Zhang, C. Zhao, X. Chen, Q. Zhang, Probing the origin of viscosity of liquid electrolytes for lithium batteries, Angew. Chem. Int. Ed. 62 (2023) e202305331, https://doi.org/10.1002/anie.202305331.

[25] P. Nie, M. Liu, W. Qu, M. Hou, L. Chang, Z. Wu, H. Wang, J. Jiang, Unravelling the solvation structure and interfacial mechanism of fluorinated localized high concentration electrolytes in K-ion batteries, Adv. Funct. Mater. 33 (2023), https://doi.org/10.1002/adfm.202302235.

[26] A.K. Arof, S. Amirudin, S.Z. Yusof, I.M. Noor, A method based on impedance spectroscopy to determine transport properties of polymer electrolytes, Phys. Chem. Chem. Phys. 16 (2014) 1856–1867, https://doi.org/10.1039/c3cp53830c.

[27] T.M.W.J. Bandara, M.A.K.L. Dissanayake, I. Albinsson, B. Mellander, Mobile charge carrier concentration and mobility of a polymer electrolyte containing PEO and Pr4N+I− using electrical and dielectric measurements, Solid State Ion 189 (2011) 63–68, https://doi.org/10.1016/j.ssi.2011.03.004.

[28] J. Zeng, L. Dong, W. Sha, L. Wei, X. Guo, Highly stretchable, compressible and arbitrarily deformable all-hydrogel soft supercapacitors, J. Chem. Eng. 383 (2020) 123098, https://doi.org/10.1016/j.cej.2019.123098.

[29] J. Bae, M.K. Song, Y.J. Park, J.M. Kim, M. Liu, Z.L. Wang, Fiber supercapacitors made of nanowire-fiber hybrid structures for wearable/flexible energy storage, Angew. Chem. Int. Ed. 50 (2011) 1683–1687, https://doi.org/10.1002/anie.201006062.

[30] P. Xu, T. Gu, Z. Cao, B. Wei, J. Yu, F. Li, J. Byun, W. Lu, Q. Li, T. Chou, Carbon nanotube fiber based stretchable wire-shaped supercapacitors, Adv. Energy Mater. 4 (2014), https://doi.org/10.1002/aenm.201300759.

[31] J. Sun, Y. Huang, C. Fu, Z. Wang, Y. Huang, M. Zhu, C. Zhi, H. Hu, High-performance stretchable yarn supercapacitor based on PPy@CNTs@urethane elastic fiber core spun yarn, Nano Energy 27 (2016) 230–237, https://doi.org/10.1016/j.nanoen.2016.07.008.

[32] X. Guan, L. Pan, Z. Fan, Flexible, transparent and highly conductive polymer film electrodes for all-solid-State transparent supercapacitor applications, Membranes 11 (2021) 788, https://doi.org/10.3390/membranes11100788.

[33] R.K. Ramakrishnan, S. Wacławek, M. Černík, V.V.T. Padil, Biomacromolecule assembly based on gum kondagogu-sodium alginate composites and their

expediency in flexible packaging films, Int. J. Biol. Macromol. 177 (2021) 526–534, https://doi.org/10.1016/j.ijbiomac.2021.02.156.
[34] R.K. Ramakrishnan, V.V.T. Padil, M. Škodová, S. Wacławek, M. Černík, S. Agarwal, Hierarchically porous bio-based sustainable conjugate sponge for highly selective oil/organic solvent absorption, Adv. Funct. Mater. 31 (2021), https://doi.org/10.1002/adfm.202100640.
[35] R.K. Ramakrishnan, V.V.T. Padil, S. Wacławek, M. Černík, D. Tiwari, Sustainable, biodegradable, and recyclable bio-sponge for rapid and practical bioremediation of dye from water, J. Environ. Chem. Eng. 10 (2022) 108285, https://doi.org/10.1016/j.jece.2022.108285.